Journal of Inorganic Biochemistry 237 (2022) 112011

Contents lists available at ScienceDirect

Journal of Inorganic Biochemistry

journal homepage: www.elsevier.com/locate/jinorgbio

Anticancer mechanism studies of iridium(III) complexes inhibiting osteosarcoma HOS cells proliferation

Fu-Li Xie [a,c,1], Yan Wang [a,c,1], Jian-Wei Zhu [a,c,1], Hui-Hua Xu [a,c], Qi-Feng Guo [a,c,*], Yong Wu [b,c,*], Si-Hong Liu [a,c,*]

[a] Department of Orthopaedics, the Second Affiliated Hospital, School of Medicine, South China University of Technology, Guangzhou, Guangdong 510180, PR China
[b] Department of Oncology, the Second Affiliated Hospital, School of Medicine, South China University of Technology, Guangzhou, Guangdong 510180, PR China
[c] Guangzhou First People's Hospital, Guangzhou, Guangdong 510180, PR China

ARTICLE INFO

Keywords:
Osteosarcoma
Iridium (III) complexes
Autophagy
Mitochondria
Antitumor
HOS cells

ABSTRACT

Three iridium (III) polypyridine complexes [Ir(bzq)$_2$(maip)](PF$_6$) (**Ir1** , bzq = benzo[*h*]quinoline, maip = 3-aminophenyl-1H-imidazo[4,5-f][1,10]phenanthroline), [Ir(bzq)$_2$(apip)](PF$_6$) (**Ir2**, apip = 2-aminophenyl-1H-imidazo[4,5-f][1,10]phenanthroline) and [Ir(bzq)$_2$(paip)](PF$_6$) (**Ir3**, paip = 4-aminophenyl-1H-imidazo[4,5-f][1,10]phenanthroline) were synthesized and characterized. The cytotoxic activities of the three complexes against human osteosarcoma HOS, U2OS, MG63 and normal LO2 cells were evaluated by MTT (3-(4,5-dimethylthiazol-2-yl)-2,5-diphenyltetrazolium bromide) method. The results showed that **Ir1**–**3** exhibited moderate antitumor activity against HOS with IC$_{50}$ of 21.8 ± 0. 4 μM,10.5 ± 1.8 μM and 7.4 ± 0.4 μM, respectively. We found that **Ir1**–**3** can effectively inhibit HOS cells growth and blocked the cell cycle at the G0/G1 phase. Further studies revealed that complexes can increase intracellular reactive oxygen species (ROS) and Ca^{2+}, which accompanied by mitochondria-mediated intrinsic apoptosis pathway. In addition, autophagy was also investigated. Taken together, the complexes induce HOS apoptosis through a ROS-mediated mitochondrial dysfunction pathway and inhibition of the PI3K (phosphatidylinositol 3-kinase)/AKT (protein kinase B)/mTOR (mammalian target of rapamycin) signaling pathway. This study provides useful help for understanding the anticancer mechanism of iridium (III) complexes toward osteosarcoma treatment.

1. Introduction

Osteosarcoma (*OS*) is the most common primary malignant bone cancer in children and young adults, with an annual incidence of between 1 and 3 cases per million worldwide [1]. The treatment of newly diagnosed osteosarcoma is a combination of preoperative and postoperative chemotherapy and surgery [2]. There is no specific chemotherapy for osteosarcoma at present. Despite the continuous improvement of new drugs, methotrexate, doxorubicin and cisplatin are still the most commonly used combination chemotherapy schemes for children and young adult patients [3,4]. Although neoadjuvant therapy and extensive tumor resection have improved survival, clinical outcomes and 5-year survival in patients with OS remain unsatisfactory due to early lung metastasis and drug resistance of the tumor [5–7]. As the first generation of anticancer drugs, cisplatin has severe toxic side effects and drug resistance which limit long-term use and clinical efficacy [8–10]. In recent years, iridium, ruthenium, rhodium, titanium and other non-platinum metal complexes have developed rapidly as substitutes for platinum organometallic anticancer drugs [11–14]. Iridium complexes are widely used as cell probes, organelle-targeted imaging reagents and tumor chemotherapy drugs because of their excellent photophysical properties, low toxicity and strong anti-tumor activity [15–22]. Zhang et al. reported that the iridium(III) complexes containing maip (3-aminophenyl-1*H*-imidazo[4,5-f][1,10]phenanthroline), apip (2-aminophenyl-1*H*-imidazo[4,5-f][1,10]phenanthroline) and paip (4-aminophenyl-1*H*-imidazo[4,5-f][1,10]phenanthroline) show high anticancer efficacy against B16 and A549 cells [18] This stimulates us to choose these ligands to synthesize iridium(III) complexes, owing to benzo[*h*]quinoline (bzq) possessing good planarity and hydrophobicity, we chose bzq as an ancillary. At present, the cancer cells including A549,

* Corresponding authors at: Department of Orthopaedics, the Second Affiliated Hospital, School of Medicine, South China University of Technology, Guangzhou, Guangdong, 510180, PR China
E-mail addresses: eyguoqf@scut.edu.cn (Q.-F. Guo), eywuyong@scut.edu.cn (Y. Wu), eyliush@scut.edu.cn (S.-H. Liu).
[1] These authors contribute equally.

https://doi.org/10.1016/j.jinorgbio.2022.112011
Received 25 March 2022; Received in revised form 14 September 2022; Accepted 14 September 2022
Available online 20 September 2022

HeLa, HepG2, BEL-7402 and SGC-7901 cells are chosen for many iridium(III) complexes, very few literatures reported the studies on osteosarcoma cells of iridium(III) complexes. Therefore, in this paper, we choose HOS, U2OS, MG63 osteosarcoma cells and investigate the antitumor effect of the iridium(III) complexes. To obtain much anticancer information and further understanding the anticancer mechanism of iridium(III) complexes, herein, three new iridium(III) complexes [Ir(bzq)$_2$(maip)](PF$_6$) (**Ir1**), [Ir(bzq)$_2$(apip)](PF$_6$) (**Ir2**) and [Ir(bzq)$_2$(paip)](PF$_6$) (**Ir3**, Scheme 1) were designed and synthesized. The complexes were characterized by HRMS,^{1}H NMR and ^{13}C NMR. The cytotoxic activity of the complexes against osteosarcoma HOS, U2OS, MG63 and normal LO2 cells was investigated by 3-(4,5-dimethylthiazol-2-yl)-2,5-diphenyltetrazolium bromide (MTT). The anticancer efficacy was evaluated by endocytosis, apoptosis, cell cycle arrest, reactive oxygen species, mitochondrial membrane potential. The expression of B-cell lymphoma-2 family proteins was explored by western blot.

2. Experimental

2.1. Materials and methods

All reagents purchased are analytically pure. The experimental water was Milli-Q ultra-pure water. The fluorescent dye kit was obtained from Beyotime Biotechnology. The human osteosarcoma cell lines HOS, U2OS and MG63 and normal human hepatocytes LO2 were obtained from the experimental center of Sun Yat-Sen university (Guangzhou, China). HOS, U2OS, MG63 and LO2 cells were cultured in Dulbecco's Modified Eagle Medium (DMEM) at 37 °C and 5% CO_2. All culture mediums were added with 10% fetal bovine serum (Gibco, USA) and 1% penicillin/streptomycin.

2.2. Synthesis of complexes

2.2.1. Synthesis of [Ir(bzq)$_2$(maip)]PF$_6$ (*Ir1*)

Maip (0.16 g, 0.5 mmol) [23] and cis-[Ir(bzq)$_2$Cl]$_2$ (0.292 g, 0.25 mmol) [24] was dissolved in a mixture of dichloromethane and methanol (45 mL, V_{CH3OH}:V_{CH2Cl2} = 1:2, *v*/v) and refluxed under argon for 6 h. After cooling, NH_4PF_6 (1.5 g) was added and stirred for 30 min. The dark red precipitate was obtained. With a mixture of CH_2Cl_2/acetone (v/v, 1:3) as eluent, neutral alumina column was used to purify the crude product and finally a yellow-brown powder was obtained. Yield: 69%. Anal. Cacld for $C_{45}H_{29}N_7IrPF_6$: C, 53.78; H, 2.91; N, 9.76%. Found: 53.95; H, 2.83; N, 9.61%. HRMS (CH_3CN): Calcd. for $C_{45}H_{29}N_7IrPF_6$: *m/z* = 860.2116 ([M-PF$_6$]$^+$), found: *m/z* = 860.2117 ([M-PF$_6$]$^+$) (Error 0.12 ppm). ^{1}H NMR (DMSO-d_6, 500 MHz): δ 9.18 (d, 2H, *J* = 8.0 Hz), 8.51 (d, 2H, *J* = 7.5 Hz), 8.09 (d, 2H, *J* = 5.5 Hz), 7.99–7.92 (m, 6H), 7.87 (d, 2H, *J* = 8.5 Hz), 7.58 (d, 3H, *J* = 8.5 Hz), 7.48–7.42 (m, 3H), 7.26–7.20 (m, 3H), 6.73 (d, 1H, *J* = 8.5 Hz), 6.32 (d, 2H, *J* = 7.5 Hz), 5.40 (s, 2H). ^{13}C NMR (DMSO-d_6, 125 MHz): 158.46, 151.28, 150.82, 150.42, 149.34, 146.32, 142.39, 139.52, 135.77, 134.21, 131.74, 131.51, 130.56, 128.81, 128.71, 126.22, 124.76, 122.34, 117.76, 116.30, 113.84.

2.2.2. Synthesis of [Ir(bzq)$_2$(apip)]PF$_6$ (*Ir2*)

Ir2 was synthesized in the same method described as **Ir1**, using apip [25] in place of maip. Yield: 64%. Anal. Cacld for $C_{45}H_{29}N_7IrPF_6$: C, 53.78; H, 2.91; N, 9.76%. Found: C, 53.61; 3.03; N, 9.88%. HRMS (CH_3CN): Calcd. for $C_{45}H_{29}N_7IrPF_6$: *m/z* = 860.2116 ([M-PF$_6$]$^+$), found: *m/z* = 860.2120 ([M-PF$_6$]$^+$) (Error 0.47 ppm). ^{1}H NMR (DMSO-d_6, 500 MHz): δ 9.13 (d, 2H, *J* = 8.0 Hz), 8.51 (d, 2H, *J* = 8.0 Hz), 8.09 (d, 2H, *J* = 4.5 Hz), 8.01–7.93 (m, 8H), 7.88 (d, 2H, *J* = 8.0 Hz), 7.58 (d, 2H, *J* = 8.0 Hz), 7.44 (t, 2H, *J* = 6.0 Hz), 7.22 (t, 2H, *J* = 7.5 Hz), 6.76 (d, 2H, *J* = 8.5 Hz), 6.32 (d, 2H, *J* = 7.0 Hz), 5.77 (s, 2H). ^{13}C NMR (DMSO-d_6, 125 MHz): 164.39, 158.45, 156.49, 153.14, 150.81, 150.39, 149.31,

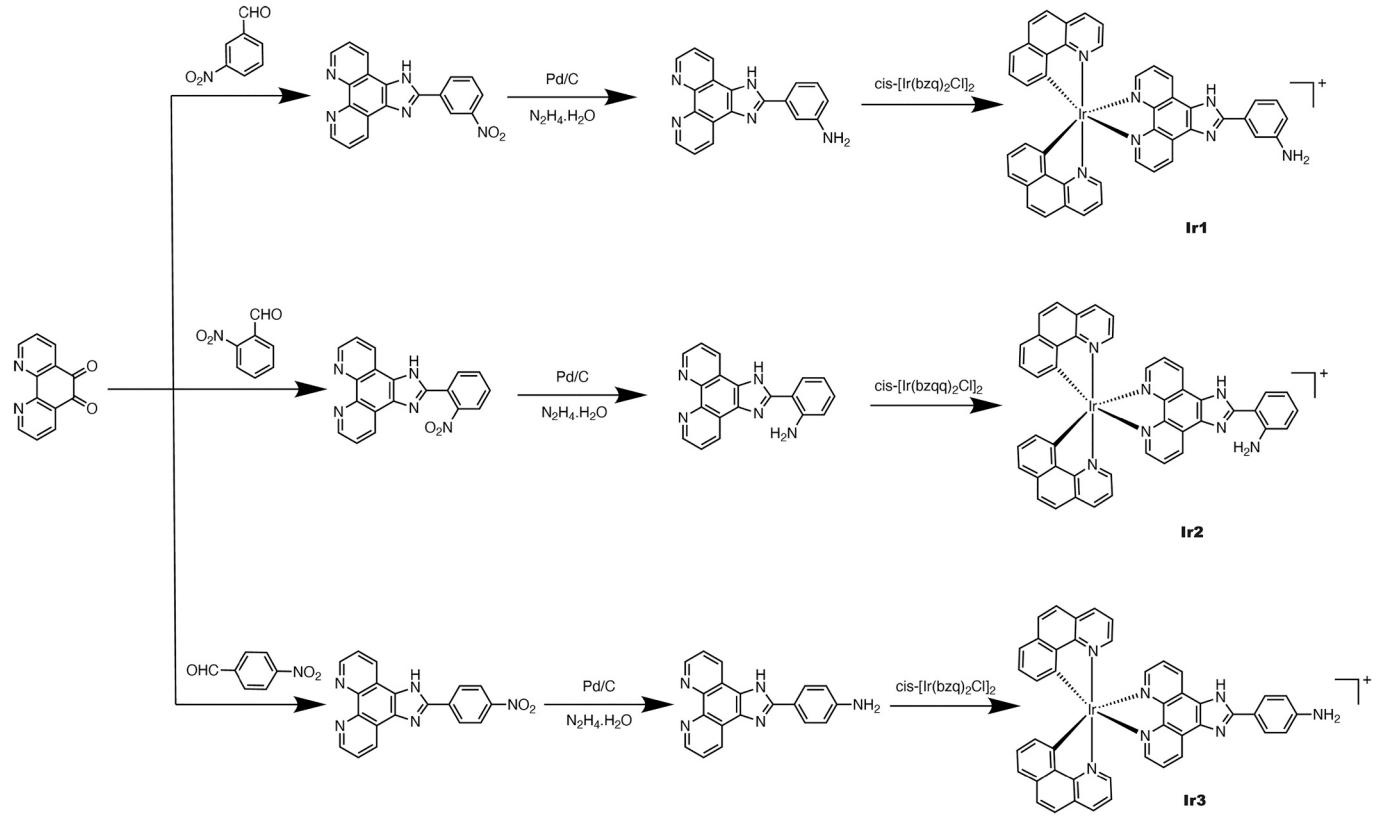

Scheme 1. Synthetic route for the complexes **Ir1**, **Ir2** and **Ir3**.

146.04, 142.38, 139.53, 135.76, 134.11, 131.75, 131.52, 130.56, 130.06, 128.76, 128.71, 126.23, 124.76, 122.36, 118.53, 115.69.

2.2.3. Synthesis of $[Ir(bzq)_2(paip)]PF_6$ (Ir3)

Ir3 was synthesized in the same method described as **Ir1**, using paip [23] in place of maip. Yield: 61%. Anal. Cacld for $C_{45}H_{29}N_7IrPF_6$: C, 53.78; H, 2.91; N, 9.76%. Found: 53.92; H, 2.78; N, 9.68%. HRMS (CH_3CN): Calcd. for $C_{45}H_{29}N_7IrPF_6$: $m/z = 860.2116$ ($[M\text{-}PF_6]^+$), found: $m/z = 860.2120$ ($[M\text{-}PF_6]^+$) (Error 0.47 ppm). ^1H NMR (DMSO-d_6, 500 MHz): δ 9.11 (d, 2H, $J = 8.5$ Hz), 8.50 (d, 2H, $J = 8.0$ Hz), 8.07 (d, 2H, $J = 5.0$ Hz), 8.01–7.91 (m, 8H), 7.87 (d, 2H, $J = 9.0$ Hz), 7.57 (d, 2H, $J = 8.0$ Hz), 7.45–7.42 (m, 2H), 7.22 (t, 2H, $J = 7.5$ Hz), 6.73 (d, 2H, $J = 8.5$ Hz), 6.31 (d, 2H, $J = 7.0$ Hz), 5.71 (s, 2H). ^{13}C NMR (DMSO-d_6, 125 MHz): 158.48, 152.86, 150.74, 150.10, 149.40, 145.87, 142.40, 139.51, 135.77, 134.03, 131.73, 131.52, 130.56, 130.01, 128.71, 128.60, 126.21, 124.75, 122.32, 115.69.

2.3. Cell viability assay

The osteosarcoma cells HOS, U2OS, MG63 and normal cells LO2 were seeded into 96-well plates at 2×10^3 cells/well. After 24 h, the cells were added with various concentrations (3.125, 6.25, 12.5, 25, 50, 100 μM) of iridium (III) complexes for 48 h. Upon completion of the incubation, DMEM (90 μL) and MTT (10 μL) was added in and the cells were incubated for 4 h at 37 °C. After the media were removed and replaced with 100 μL DMSO (final concentration of 0.05%). The absorbance was determined at 490 nm using a microplate reader. The experiment was repeated three times independently and the mean value was calculated.

2.4. Cell uptake analysis

HOS cells were inoculated into 12-well plates and incubated overnight in an incubator. When the density of each well reaches 40–50%, IC_{50} concentrations of **Ir1**, **Ir2** and **Ir3** were added into the cells and incubated for 24 h. The cells were washed twice with PBS and incubated with 75% ethanol (300 μL/well) for 20 min. The samples were observed under fluorescence microscope.

The cell uptake was quantitatively determined by inductively coupled plasma-mass spectrometry (ICP-MS, Thermo Fisher Scientific iCAP Qc) according to the literature [26]. HOS cells (5.0×10^4 cells/well) were seeded in 6-well plate and incubated with 20.0 μM of **Ir1**, **Ir2** and **Ir3** for 8 h when the cells arrived logarithmic phase. Then, washing the adherent cells twice with PBS containing 5 mM EDTA. After trypsinization and centrifugation of the suspension at 800 rpm for 5 min, repeating the above processes till the residual complexes were completely removed. The cells were digested with 60% HNO_3 at 60 °C to completely release the endocytosed iridium(III) complexes from the cells and then a 5 mL solution was obtained by adding Milli-Q water. The endocytosed mounts were calculated through the following procedures: (I) determining the intensity (^{193}Ir) of different concentrations of iridium standard solution, through linear fitting to obtain a fitting equation (x-axis: concentration of sample; y-axis: intensity). (II) determining the intensity (^{193}Ir) in the sample, then calculate the uptake amount according to the fitting equation.

2.5. Cell cloning experiment

HOS cells (700 cells/well) were cultured into 6-well plates overnight. The cells were treated with IC_{50} concentrations of **Ir1**, **Ir2** and **Ir3** and incubated for 48 h. The culture medium was removed every two days and continuously cultured for one week. After washing with PBS, the cells were stained with 0.1% (*w/v*) crystal violet and observed under a fluorescence microscope.

2.6. Cell cycle analysis

HOS cells (1×10^5 cells per well) were seeded at in 6-well plates overnight. Then the cells were exposed to IC_{50} concentrations of **Ir1**, **Ir2** and **Ir3** for 24 h. The cells were fixed with 70% ethanol at 4 °C overnight, and subsequently stained with propidium iodide (PI) for 15 min in the dark. The cell cycle distribution was detected by flow cytometry.

2.7. Apoptosis assay

HOS cells were grown in six-well plates and then treated with IC_{50} concentrations of **Ir1**, **Ir2** and **Ir3** for 24 h. Afterwards, the cells were washed three times with phosphate buffer saline (PBS) and resuspended in 195 μL of buffer. The cells were dyed with 5 μL Annexin V-FITC (fluorescein isothiocyanate) and 10 μL propidium iodide (PI) for 20 min in the dark at room temperature. The apoptotic percentage in the cells was measured by flow cytometry.

2.8. Intracellular ROS level assays

Intracellular reactive oxygen species (ROS) generation was measured using a dichlorofluorescein diacetate (DCFH-DA) assay kit according to the manufacturer's instructions. Briefly, after HOS cells were treated with IC_{50} concentrations of **Ir1**, **Ir2** and **Ir3** for 24 h, the cells were harvested and then stained with 200 μL DCFH-DA solution for 30 min at 37 °C. After rinsed twice, the cells were imaged under a fluorescence microscope and the fluorescence intensity of dichlorofluorescein (DCF) was examined to assess intracellular ROS level.

2.9. Lysosomal localization assay

HOS cells (6×10^4 cells per well) were cultured on 12-well plates overnight. After 4 h incubation with IC_{50} concentrations of **Ir1**, **Ir2** and **Ir3**, the cells were stained with LysoTracker Red at 37 °C for 30 min. Then the cells were observed under a fluorescence Microscope.

2.10. Autophagy

After the HOS cells were treated with IC_{50} concentrations of **Ir1**, **Ir2** and **Ir3** for 24 h, the cells were washed with PBS twice, and stained with 50 μM dansylcadaverine (MDC) at 37 °C for 25 min. Then the cells were washed with PBS twice and the cells was photographed under a fluorescence microscope.

2.11. Measurement of intracellular Ca^{2+}

The levels of intracellular Ca^{2+} were measured using the Fluo-3-pentaacetoxymethyl ester (Fluo-3 AM) fluorescent dye (Beyotime, Guangzhou) according to the manufacture's instruction. HOS cells were treated with IC_{50} concentrations of **Ir1**, **Ir2** and **Ir3** for 24 h, and the cells were dyed with Fluo-3 AM at 37 °C for 25 min in darkness. Then the cells were washed twice times with PBS, the cells were observed under fluorescence microscopy.

2.12. Localization of the complexes at the mitochondria

HOS cells were incubated in a six-well plate overnight, the cells were exposed to IC_{50} concentrations of **Ir1**, **Ir2** and **Ir3** for 5 h. After incubation, the cells were washed twice with PBS and dyed at 37 °C for 30 min. The residual dye was then washed with PBS, and the cells were observed under a fluorescence microscope.

2.13. Detection of mitochondrial membrane potential (MMP)

HOS cells (6×10^4 cells per well) were plated in 12-well plate overnight, and then the cells were treated with IC_{50} concentrations of

Ir1, **Ir2** and **Ir3** for 24 h. Next, the cells were harvested and dyed with 1 μg/mL of JC-1 (5,5′,6,6′-tetrachloro-1,1′,3,3′-tetraethyl-imidacarbocyanineiodide) for 30 min at room temperature. After washed twice with PBS, the cells were observed under a fluorescence microscope.

2.14. Western blotting analysis

HOS cells were harvested after the treatment with IC_{50} concentrations of **Ir1**, **Ir2** and **Ir3** for 24 h and total proteins from the cells were extracted. Protein concentrations were determined using the bicinchoninic acid (BCA) method. Proteins separated by sodium dodecyl sulfate polyacrylamide gel electrophoresis (SDS-PAGE) were transferred onto polyvinylidene difluoride (PVDF) membranes, which were blocked with 5% non-fat milk for 3 h. The membranes were incubated with primary antibodies overnight at 4 °C and then were probed with secondary antibody for 70 min at room temperature. Immunoblot signals were visualized with enhanced chemiluminescence.

3. Results and discussion

3.1. Synthesis and characterization

The ligands maip, apip and paip were prepared according to the literature. The complexes **Ir1**, **Ir2** and **Ir3** were synthesized by the direct reaction with ligands and $[Ir(bzq)_2Cl]_2$ in dichloromethane and methanol. The complexes were purified by neutral alumina column using CH_2Cl_2/acetone as eluent. In the HRMS spectra, the determined molecular weights are consistent with the expected values. In the ^1H NMR spectra, the peaks of 5.40 for **Ir1**, 5.77 for **Ir2** and 5.71 ppm for **Ir3** are assigned to the hydrogen atoms in the -NH_2. The complexes can be dissolved in CH_3OH, CH_3CH_2OH, CH_2Cl_2 and DMSO. The UV–Vis and luminescence spectra of the complexes in PBS solution was determined. As shown in **Fig. S1a** and **S1b (supporting information)**, complexes **Ir1**, **Ir2** and **Ir3** show one distinct band at 261 (ε = 20,300), 259 (ε = 32,500), 258 nm (ε = 30,950), respectively. The range of the emission spectra of the complexes is 580–610 nm, and the emission maxima of complexes **Ir1**-**Ir3** appeared at 598 nm (λ_{ex} = 295 nm), 595 nm (λ_{ex} = 295 nm) and 596 nm (λ_{ex} = 295 nm), respectively.

3.2. Cytotoxic activity in vitro studies

The in vitro cytotoxicity of the complexes **Ir1**, **Ir2** and **Ir3** against HOS, U2OS, MG63 and LO2 was investigated by MTT assay (3-(4,5-dimethylthiazol-2-yl)-2,5-diphenyl tetrazolium bromide) [27]. The results of the antitumor activity of these complexes against selected tumor cell lines compared to cisplatin are shown in Table 1. The complexes exhibited moderate cytotoxic activity against the selected cancer cells. In addition, the complex $[Ir(bzq)_2(paip)](PF_6)$ (**Ir3)** show lower cytotoxic activity than the complex $[Ir(piq)_2(paip)](PF_6)$ (piq = 1-phenylisoquinoline, $IC_{50} = 4.7 \pm 0.2$ μM) [18] against HepG2 cells. Comparing complexes $[Ir(bzq)_2(paip)](PF_6)$ and $[Ir(piq)_2(paip)](PF_6)$, the two complexes containing the same main ligand paip and different ancillary ligands (bzq or piq), the difference in the cytotoxic activity toward HepG2 cells may be caused by different ancillary ligands. The cytotoxic activity of **Ir1**, **Ir2** and **Ir3** is higher than that of complex VO(*od*)phen (IC_{50} = 58 μM, od = oxodiacetate, phen = 1,10-phenanthroline) [28] and Ru(II) complex $[Ru(dmp)_2(dcdppz)](ClO_4)_2$ ($IC_{50} = 22.51 \pm 1.35$ μM, dmp = 2,9-dimethyl-1,10-phenanthroline, dcdppz = 7,8-dichlorodipyrido[3,2-*a*:2′,3′-*c*]phenazine) [29] against MG63 cells. Although the complexes show markedly higher activity than cisplatin toward MG63 cells, we found that many literatures reported that osteosarcoma MG63 cells were used as research subject [30–32], few literatures reported the anticancer effect on the compound on osteosarcoma HOS cells, and the IC_{50} values of complexes **Ir1**, **Ir2** and **Ir3** toward HOS cells are lower than toward MG63 cells, therefore, in this paper, we chose HOS cell to undergo the following cell experiments.

Table 1
IC_{50} values (μM) of the cisplatin and complexes toward the selected cancer cells for 48 h.

Complexes	HOS	U2OS	MG63	HepG2	LO2
Ir1	21.8 ± 0.4	27.8 ± 1.3	31.1 ± 1.3	95.5 ± 6.6	> 100
Ir2	10.5 ± 1.8	28.3 ± 2.9	19.5 ± 0.3	> 200	> 100
Ir3	7.4 ± 0.4	9.5 ± 0.7	9.5 ± 0.7	15.1 ± 1.0	32.5 ± 1.5
cisplatin	7.8 ± 0.5	8.8 ± 0.1	48.7 ± 2.0	12.2 ± 1.4	18.7 ± 0.7

3.3. Assay of cellular uptake of complexes

After uptake by the cell, the complexes can accumulate in the different subcellular structures of the cell. The intracellular uptake level was detected by fluorescence technique to investigate the relationship between uptake level and antitumor activity. As shown in Fig. 1a, we found that the complexes can enter to the cells and emit green fluorescence compared to the blank group. To compare the amount of the complexes entering the cells, the green fluorescence intensity was quantified by flow cytometry. As shown in Fig. 1b, after HOS cells were exposed to IC_{50} concentrations of **Ir1**, **Ir2** and **Ir3** for 24 h, the fluorescence intensity increases by 6.76, 1.57 and 1.46 times for **Ir1**, **Ir2** and **Ir3** compared to that in the control. These results indicate that the complexes were successfully endocytosed. In addition, we use inductively coupled plasma-mass spectrometry (ICP-MS) to quantitatively determine the amounts of the complexes entering the cells. After 8 h of exposure of HOS cells with 20.0 μM of the complexes, the amounts of the complexes entering the cells are 103.94 ± 6.11, 4.26 ± 0.14 and 5.95 ± 0.45 ng/10^6 cells for **Ir1**, **Ir2** and **Ir3**, respectively. The amounts of the complexes entering the cells are not consistent with the cytotoxic activity of the complexes against HOS cells.

3.4. Colony formation assays

Excessive proliferation and invasion of tumor cells are hallmarks of cancer [33]. To evaluate the effect of complexes on osteosarcoma cell proliferation, the colony formation assay was investigated. As shown in **Fig. S2 (supporting information)**, the cells in the control grew rapidly, and large colony distribution was observed under the microscope after crystal violet staining. However, after HOS cells were treated with IC_{50} concentrations of **Ir1**, **Ir2** and **Ir3**, the number of colonies of cells was significantly reduced. The results show that complexes **Ir1**, **Ir2** and **Ir3** can significantly inhibit the proliferation of HOS cells.

3.5. Effect of complexes on cell cycle distribution

Cell proliferation inhibition or death is the result of apoptosis, cell cycle arrest, or both [34–36]. To explore the mechanism of the complexes inhibiting the cell proliferation, the cell cycle arrest was studied by flow cytometry. As shown in Fig. 2, in the control, the percentage in the cell at G0/G1 phase is 35.19%. After a 24 h treatment of HOS cells (a) with IC_{50} concentrations of **Ir1** (b), **Ir2** (c) and **Ir3** (d), the percentage in the cells at G0/G1 phase increased by 5.68%, 16.85% and 20.67% compared to that in the control. Obviously, complexes **Ir2** and **Ir3** show higher efficacy on the cell cycle arrest than **Ir1** under the same conditions. These results indicated that **Ir1–3** inhibit the cell growth at G0/G1 phase.

3.6. *Ir1–3* promote cell apoptosis

Apoptosis, known as programmed death, exhibits early phosphatidylserine externalization and can be detected by staining with the phospholipid-binding protein Annexin V and PI [37,38]. To evaluate the effect of the complexes on apoptosis, the apoptosis was investigated by flow cytometry. As shown in Fig. 3, Q2, Q3 and Q4 stand for late

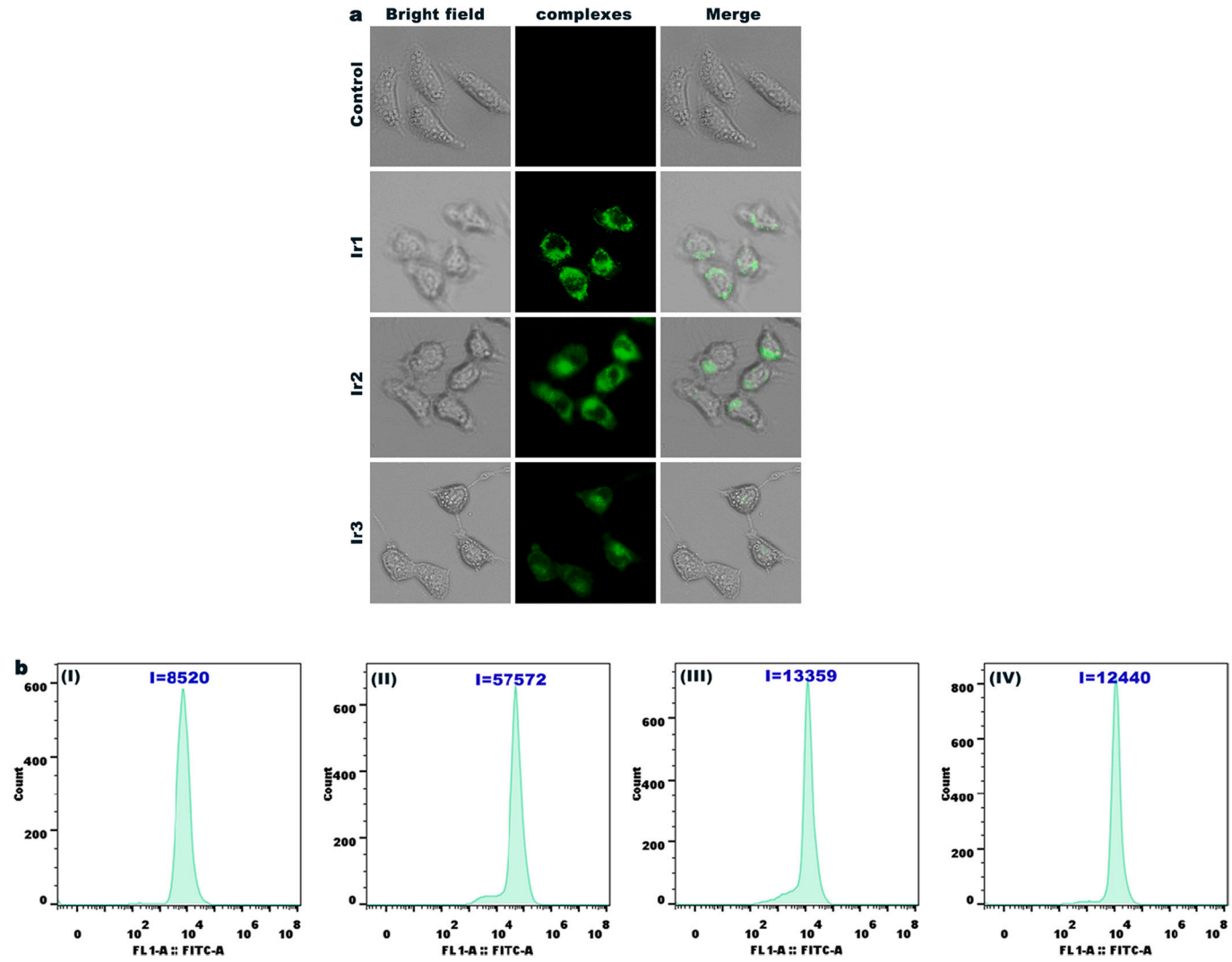

Fig. 1. (a) The cell uptake was observed under a fluorescence microscope after HOS cells were exposed to IC_{50} concentrations of **Ir1**, **Ir2** and **Ir3** for 24 h. (b) After incubation with IC_{50} concentrations of **Ir1** (II), **Ir2** (III) and **Ir3** (IV) for 24 h, the fluorescence intensity in HOS cells (I) was measured by flow cytometry.

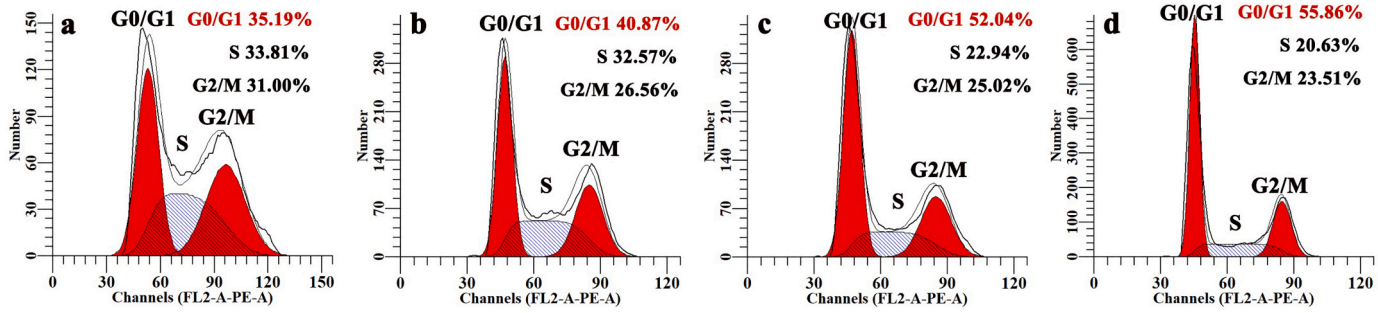

Fig. 2. Cell cycle distribution assay of HOS cells (a) treated with IC_{50} concentrations of **Ir1** (b), **Ir2** (c) and **Ir3** (d) for 24 h.

apoptosis, early apoptosis and living cells, respectively. The apoptosis rate was quantified by the sum of early and late apoptosis. In the control, the apoptotic rate is 4.66%. After HOS cells (a) were exposed to IC_{50} concentrations of cisplatin (b), **Ir1** (c), **Ir2** (d) and **Ir3** (e) for 24 h, the apoptotic rates increased by 7.73, 4.67, 6.90 and 9.15%, respectively. The apoptotic efficacy follows the order of **Ir3** > cisplatin > **Ir2** > **Ir1**. This is line with those of cytotoxic activity of the complexes against HOS cells, **Ir3** exhibits higher apoptotic effect than cisplatin. These results demonstrated that the complexes can cause apoptosis in HOS cells.

3.7. Reactive oxygen species (ROS) determination

Intracellular reactive oxygen species (ROS) are mainly produced in mitochondria, and oxidative stress caused by ROS accumulation triggers physiological disorders and cellular damage and plays a key role in tumor cell apoptosis [39–41]. The changes of intracellular ROS induced by the complexes were assessed using 2′,7′-dichlorodihydrofluorescein diacetate (DCFH-DA) as fluorescence probe. As seen from **Fig. S3a (supporting information)**, after a 24 h treatment of HOS cells (I) with

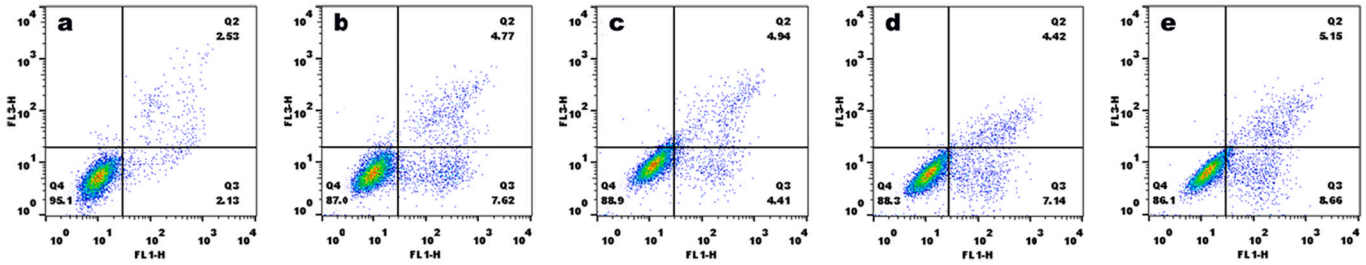

Fig. 3. Apoptosis analysis of HOS cells (a) exposure to cisplatin (b) and IC_{50} concentrations of **Ir1** (c), **Ir2** (d) and **Ir3** (e) for 24 h.

IC_{50} concentrations of **Ir1** (II), **Ir2** (III) and **Ir3** (IV) for 24 h, the green fluorescence obviously increases compared with that in the control, indicating that **Ir1–3** enhance the intracellular ROS levels. The quantification of intracellular fluorescence intensity was performed by flow cytometry. As shown in **Fig. S3b (supporting information)**, the green fluorescence increased by 1.43 times for Rosup (positive control, II), 4.47 times for **Ir1** (III), 2.99 times for **Ir2** (IV) and 2.29 times for **Ir3** (V) compared with that in the control (I). This further confirms that the complexes can increase intracellular ROS levels.

3.8. Location of the complexes at the lysosomes and autophagy

Lysosomes are degrading organelles containing acidic hydrolases whose primary role is the degradation and recycling of extracellular substances through endocytosis and phagocytosis [42,43]. Autophagy is the process in which cells are stimulated to engulf their cytoplasm or organelles and finally degrade the engulfed cells in lysosomes [44,45]. As shown in **Fig. S4a (supporting information)**, after 4 h of HOS cells exposure to IC_{50} concentrations of **Ir1**, **Ir2** and **Ir3**, the lysosomes were stained red, the complexes emit green fluorescence. The overlap of red and green fluorescence indicates that the complexes enter the

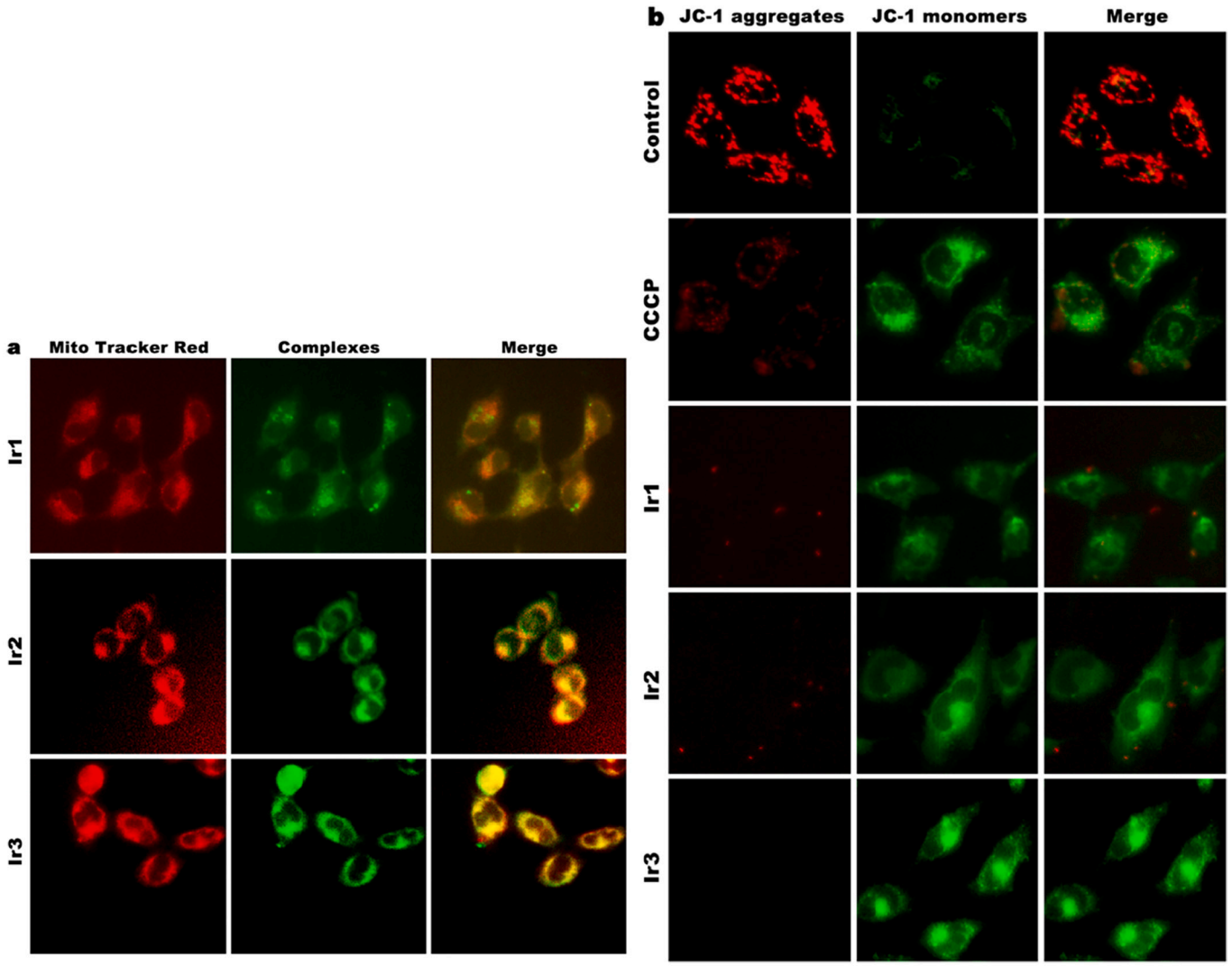

Fig. 4. (a) Colocalization of HOS cells incubated with **Ir1**, **Ir2** and **Ir3** for 5 h. (b) Assay of the change of mitochondrial membrane potential after HOS cells were treated with IC_{50} concentration of **Ir1**, **Ir2** and **Ir3** for 24 h.

lysosomes. On the other hand, MDC is commonly used as a fluorescent probe to detect autophagy. As shown in **Fig. S4b (supporting information)**, HOS cells (I) were treated with IC_{50} concentrations of **Ir1** (II), **Ir2** (III) and **Ir3** (IV) for 24 h, a number of autophagic vacuoles were observed, which suggests that the complexes can cause autophagy.

3.9. Determination of intracellular Ca^{2+} concentration

Mitochondria are one of the subcellular organelles involved in the regulation of intracellular calcium ion signaling. When large amounts of Ca^{2+} accumulate in mitochondria, the pro-apoptotic factor caspase-3 and the death-related factor poly ADP-ribose polymerase (PARP-1) are activated, which in turn induce apoptosis [46–48]. The calcium fluorescent probe Fluo-3 AM was used to detect intracellular Ca^{2+}concentration. As shown in **Fig. S5a (supporting information)**, comparing with the control, the treatment of HOS cells with IC_{50} concentrations of **Ir1**, **Ir2** and **Ir3** leads to an increase of green fluorescence intensity. The green fluorescence intensity was quantitatively determined by flow cytometry. As shown in **Fig. S5b** (supporting information), the green fluorescence intensity increases by 1.34 times for **Ir1**, 1.63 times for **Ir2** and 1.09 times for **Ir3**, respectively. The efficacy of the complexes on intracellular Ca^{2+} level follows the order of **Ir2** > **Ir1** > **Ir3**. These results indicates that the complexes can increase intracellular Ca^{2+} concentration.

3.10. Subcellular localization and membrane potential detection

Mitochondria play an important role as organelles in individual life activities and are involved in the regulation of normal cell signaling [49]. To detect whether the complexes inhibit tumor cell proliferation and induce apoptosis through mitochondrial dysfunction pathway, the location of the complexes at the mitochondria was studied. As seen in Fig. 4a, mitochondria are stained red, the complexes emit green fluorescence, the overlap of red and green fluorescence indicates that the complexes locate at the mitochondria and can damage mitochondrial dysfunction. Hence, the complexes locate at both lysosomes and mitochondria, moreover, we used ICP-MS to determine the distribution of the **Ir1** at the lysosomes and mitochondria. After the HOS cells were exposed to 20.0 μM of **Ir1** for 5 h, the distribution of **Ir1** at the lysosomes and mitochondria is 12.65 ± 2.31 and 8.57 ± 1.34 ng/10^6 cells, respectively. The results demonstrate that the complexes prefer to accumulate at the lysosomes. The increase of intracellular ROS levels induces a rapid depolarization of the inner mitochondrial membrane potential (MMP). The decrease in mitochondrial membrane potential is a hallmark event in the early stages of apoptosis [50–53]. The mitochondrial membrane potential was assessed using 5,5′,6,6′-Tetrachloro-1,1′,3,3′-tetraethylimidacarbocyanine iodide (JC-1) as a fluorescent probe. As shown in Fig. 4b, JC-1 in the control group emitted bright red fluorescence corresponding to a high MMP. In contrast, HOS cells were exposed to the carbonylcyanide-*m*-chlorophenylhydrazone (CCCP, positive control) and IC_{50} concentration of **Ir1–3**, JC-1 exhibit a lot of green fluorescence and a little of red fluorescence points corresponding to a low MMP. The results demonstrate that the complexes cause a decrease of MMP. In summary, complexes-triggered oxidative stress causes Ca^{2+} release and induced apoptosis through mitochondrial membrane depolarization.

3.11. Effects of complexes on the expression of Bcl-2 family proteins

To investigate the mechanism of **Ir1–3** inducing cancer cell death, we treated HOS cells with IC_{50} concentration of **Ir1**, **Ir2** and **Ir3** for 24 h and examined the expression levels of apoptosis-related proteins. The B-cell lymphoma-2 (Bcl-2) family proteins play a critical dual regulatory role between autophagy and mitochondrial apoptosis [54,55]. As shown in Fig. 5, the results showed that the expression of anti-apoptotic protein Bcl-2 was decreased compared to the control. Caspase-3 is an important pro-apoptotic regulator and PARP acts as a substrate for caspase-3

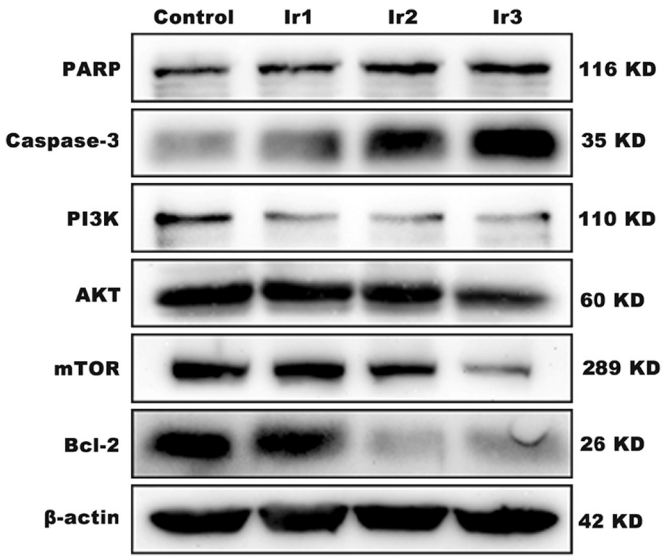

Fig. 5. The expression of Bcl-2 family protein was assayed after an exposure of HOS cells to IC_{50} concentration of **Ir1**, **Ir2** and **Ir3** for 24 h. β-actin was used as internal control.

[56–58]. The expression of PARP and apoptotic execution factor caspase-3 was significantly up-regulated in the **Ir1–3**-treated cells. The PI3K (phosphatidylinositol 3-kinase)/AKT (protein kinase B)/mTOR (mammalian target of rapamycin) pathway is an important intracellular signaling pathway. It plays an integral role in abnormal cell growth, tumor invasion and chemoresistance, and is considered an attractive therapeutic target for osteosarcoma [59,60]. The PI3K/AKT/mTOR pathway is involved in regulating mitochondrial activity and ROS production, it also is an important pathway for autophagy [61–63]. The results from the western blotting indicate that complexes **Ir1**, **Ir2** and **Ir3** inhibit the expression of PI3K, AKT and mTOR. Hence, we consider that **Ir1–3** induce apoptosis through inhibition of PI3K/AKT/mTOR pathway.

4. Conclusions

In this study, three iridium (III) complexes were synthesized and characterized. Their antitumor properties were studied. we observed that **Ir1–3** can inhibit HOS cells proliferation, induce cell cycle arrest at G0/G1 phase. At the same time, **Ir1–3** locate at the mitochondria and cause a decrease of mitochondrial membrane potential. The complexes also locate at the lysosomes and induce autophagy. Additionally, the complexes can increase intracellular ROS and Ca^{2+} levels, down-regulate the expression of Bcl-2 protein, simultaneously, up-regulate the expression of PARP and caspase 3, inhibit the expression of PI3K, AKT and mTOR (**Fig. 6**). In conclusion, the complexes induce apoptosis via a ROS-mediated mitochondrial dysfunction pathway and inhibition of PI3K/AKT/mTOR signaling pathway. This work is helpful for design and synthesis of new iridium (III) complexes as potent anti-osteosarcoma drugs.

Author statement

We declare that this manuscript has been finished by all authors listed in this manuscript, and all data are original and real. We agree to be accountable for all aspects of the work.

All authors have read this manuscript and approved the manuscript to be submitted to JIB.

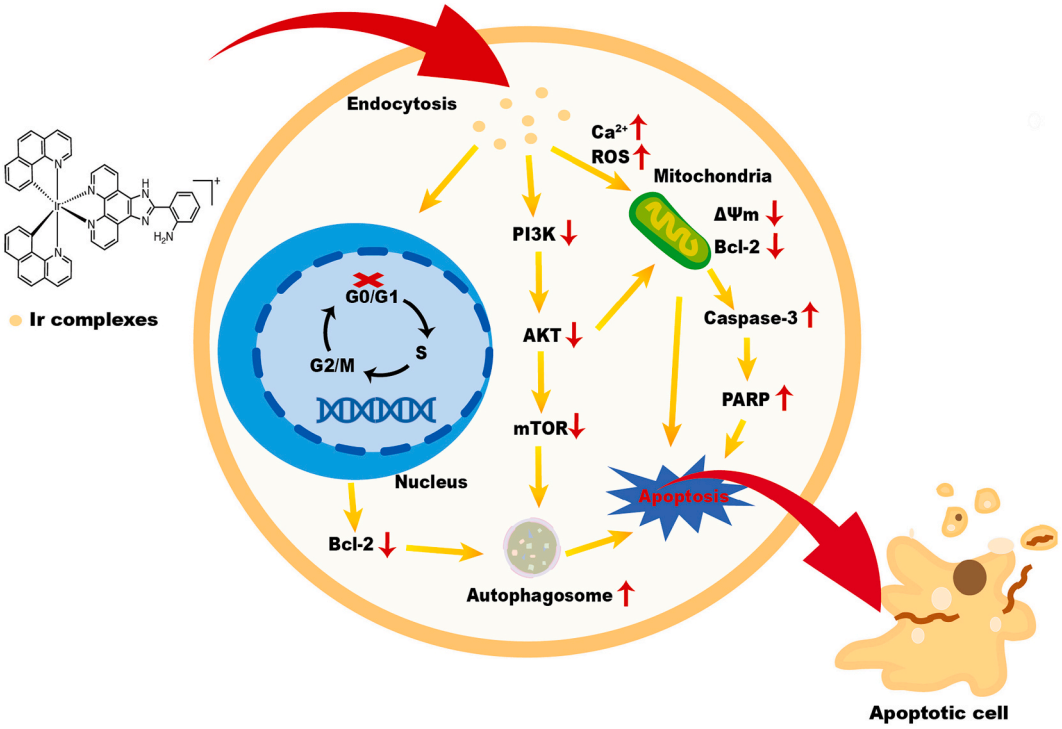

Fig. 6. The mechanism of the complexes inducing apoptosis in HOS cells.

Declaration of Competing Interest

The authors have declared that no competing interest exists.

Data availability

Data will be made available on request.

Acknowledgements

The present study was supported by National Natural Science Foundation of China (31601031, 31971164), Guangdong Special Fund Project of Fundamental and Applied Research (2022A1515012332), Guangzhou Planned Project of Science and Technology (202102010032), and the Science Foundation of Guangzhou First People's Hospital (Q2019019).

Appendix A. Supplementary data

Supplementary data to this article can be found online at https://doi.org/10.1016/j.jinorgbio.2022.112011.

References

[1] M. Kansara, M.W. Teng, M.J. Smyth, D.M. Thomas, Nat. Rev. Cancer 14 (2014) 722–735.
[2] A.J. Chou, D.S. Geller, R. Gorlick, Paediatr. Drugs 10 (2008) 315–327.
[3] M.S. Isakoff, S.S. Bielack, P. Meltzer, R. Gorlick, J. Clin. Oncol. 33 (2015) 3029–3035.
[4] S.S. Bielack, S. Hecker-Nolting, C. Blattmann, L. Kager, F1000Res 5 (2016) 2767.
[5] S.S. Bielack, B. Kempf-Bielack, G. Delling, G.U. Exner, S. Flege, K. Helmke, R. Kotz, M. Salzer-Kuntschik, M. Werner, W. Winkelmann, A. Zoubek, H. Jürgens, K. Winkler, J. Clin. Oncol. 20 (2002) 776–790.
[6] E. Ward, C. DeSantis, A. Robbins, B. Kohler, A. Jemal, CA Cancer J. Clin. 64 (2014) 83–103.
[7] B. Kempf-Bielack, S.S. Bielack, H. Jürgens, D. Branscheid, W.E. Berdel, G.U. Exner, U. Göbel, K. Helmke, G. Jundt, H. Kabisch, M. Kevric, T. Klingebiel, R. Kotz, R. Maas, R. Schwarz, M. Semik, J. Treuner, A. Zoubek, K. Winkler, J. Clin. Oncol. 23 (2005) 559–568.
[8] E. Wiltshaw, Platin. Met. Rev. 23 (1979) 90–98.
[9] M. Chovanec, M. Abu Zaid, N. Hanna, N. El-Kouri, L.H. Einhorn, C. Albany, Ann. Oncol. 28 (2017) 2670–2679.
[10] V. Brabec, J. Kasparkova, Drug Resist. Updat. 8 (2005) 131–146.
[11] Q. Sun, Y. Wang, Q. Fu, A. Ouyang, S. Liu, Z. Wang, Z. Su, J. Song, Q. Zhang, P. Zhang, D. Lu, Angew. Chem. Int. Ed. Eng. 60 (2021) 4841–4848.
[12] Z.Y. Liu, J. Zhang, Y.M. Sun, C.F. Zhu, Y.N. Lu, J.Z. Wu, J. Li, H.Y. Liu, Y. Ye, J. Mater. Chem. B 8 (2020) 438–446.
[13] J. Wang, J.J. Nie, P. Guo, Z. Yan, B. Yu, W. Bu, J. Am. Chem. Soc. 142 (2020) 2709–2714.
[14] G. Lan, K. Ni, S.S. Veroneau, X. Feng, G.T. Nash, T. Luo, Z. Xu, W. Lin, J. Am. Chem. Soc. 141 (2019) 4204–4208.
[15] S.M. King, S. Claire, R.I. Teixeira, A.N. Dosumu, A.J. Carrod, H. Dehghani, M. J. Hannon, A.D. Ward, R. Bicknell, S.W. Botchway, N.J. Hodges, Z. Pikramenou, J. Am. Chem. Soc. 140 (2018) 10242–10249.
[16] Q. Chen, C. Jin, X. Shao, R. Guan, Z. Tian, C. Wang, F. Liu, P. Ling, J.L. Guan, L. Ji, F. Wang, H. Chao, J. Diao, Small 14 (2018), e1802166.
[17] S. Kuang, X. Liao, X. Zhang, T.W. Rees, R. Guan, K. Xiong, Y. Chen, L. Ji, H. Chao, Angew. Chem. Int. Ed. Eng. 59 (2020) 3315–3321.
[18] Y.Y. Zhang, Y. Zhou, H.W. Zhang, L. Tian, J. Hao, Y.H. Yuan, W.L. Li, Y.J. Liu, J. Inorg. Biochem. 224 (2021), 111580.
[19] Y. Zhou, L. Bai, L. Tian, L.L. Yang, H.W. Zhang, Y.Y. Zhang, J. Hao, Y.Y. Gu, Y. J. Liu, J. Inorg. Biochem. 223 (2021), 111550.
[20] F.L. Xie, Z.Z. Huang, L. Bai, J.W. Zhu, H.H. Xu, Q.Q. Long, Q.F. Guo, Y. Wu, S. H. Liu, J. Inorg. Biochem. 225 (2021), 111603.
[21] I. Echevarra, E. Zafon, S. Barrabés, M.A. Martíne, S. Romas-Gómez, N. Ortega, B. R. Manzano, E.A. Jalón, R. Quesada, G. Espino, A. Massaguer, J. Inorg. Biochem. 231 (2022), 111790.
[22] Y.H. Yuan, C.L. Shi, X.Y. Wu, W.L. Li, C.X. Huang, L.J. Liang, J. Chen, Y. Wang, Y. J. Liu, J. Inorg. Biochem. 232 (2022), 111820.
[23] H.L. Huang, Y.J. Liu, C.H. Zeng, L.X. He, F.H. Wu, DNA Cell Biol. 29 (2010) 261–270.
[24] S. Sprouse, K.A. King, P.J. Spellane, R.J. Watts, J. Am. Chem. Soc. 106 (1984) 6647–6653.
[25] Z.H. Liang, Z.Z. Li, H.L. Huang, Y.J. Liu, J. Coord. Chem. 64 (2011) 3342–3352.
[26] W.L. Li, C.L. Shi, X.Y. Wu, Y.Y. Zhang, H.M. Liu, X.Z. Wang, C.X. Huang, L.J. Liang, Y.J. Liu, J. Inorg. Biochem. 236 (2022), 111977.
[27] T. Mosmann, J. Immunol. Methods 65 (1983) 55–63.
[28] I.E. León, N. Butenko, A.L.D. Virgilio, C.I. Muglia, E.J. Baran, I. Cavaco, S. B. Etcheverry, J. Inorg. Biochem. 134 (2014) 106–117.
[29] H.L. Huang, Z.Z. Li, Z.H. Liang, Y.J. Liu, Eur. J. Inorg. Chem. 2011 (2011) 5538–5547.
[30] E. Blanchet, M. Vansteelandt, R. Le Bot, M. Egorow, Y. Guitton, Y.F. Pouchus, O. Grovel, Eur. J. Med. Chem. 79 (2014) 244–250.
[31] S.Q. Zhang, H. Ren, H.T. Sun, S.H. Cao, Saudi, J. Biol. Sci. 28 (2021) 4908–4915.
[32] Y.D. Qin, F.M. Fang, J.J. Zhou, R.B. Wang, S.X. Xu, L.H. Li, H.L. Zhang, Fitoterapia 146 (2020), 104727.
[33] D. Hanahan, R.A. Weinberg, Cell 144 (2011) 646–674.

[34] S.M. Wang, J. Pang, K.J. Zhang, Z.Y. Zhou, F.Y. Chen, Mol. Ther. Oncolytics 21 (2021) 62–73.
[35] T. Liang, X. Ye, Y. Liu, X. Qiu, Z. Li, B. Tian, D. Yan, Exp. Mol. Med. 50 (2018) 1–12.
[36] M. Malumbres, M. Barbacid, Nat. Rev. Cancer 9 (2009) 153–166.
[37] S. Jitkaew, A. Trebinska, E. Grzybowska, G. Carlsson, A. Nordström, J. Lehtiö, A. S. Fröjmark, N. Dahl, B. Fadeel, J. Biol. Chem. 284 (2009) 27827–27837.
[38] S. Kesavardhana, R.K.S. Malireddi, T.D. Kanneganti, Annu. Rev. Immunol. 38 (2020) 567–595.
[39] R.P. Chakrabarty, N.S. Chandel, Cell Stem Cell 28 (2021) 394–408.
[40] H. Sies, D.P. Jones, Nat. Rev. Mol. Cell Biol. 21 (2020) 363–383.
[41] V.N. Kotiadis, M.R. Duchen, L.D. Osellame, Biochim. Biophys. Acta Gen. Subj. 1840 (2014) 1254–1265.
[42] F. Wang, R. Gómez-Sintes, P. Boya, Traffic 19 (2018) 918–931.
[43] S.R. Bonam, F. Wang, S. Muller, Nat. Rev. Drug Discov. 18 (2019) 923–948.
[44] N. Mizushima, Genes Dev. 21 (2007) 2861–2873.
[45] J.M.M. Levy, C.G. Towers, A. Thorburn, Nat. Rev. Cancer 17 (2017) 528–542.
[46] T. Pathak, M. Trebak, Pharmacol. Ther. 192 (2018) 112–123.
[47] Z. Xia, C. Wang, X. Wang, H. Yu, H. Yao, H. Shen, X. Lan, X. Wu, G. Zhang, Toxicol. in Vitro 72 (2021), 105104.
[48] H. Wang, N. Zhai, Y. Chen, H. Xu, K. Huang, J. Inorg. Biochem. 172 (2017) 16–22.
[49] F.J. Bock, S.W.G. Tait, Nat. Rev. Mol. Cell Biol. 21 (2020) 85–100.
[50] H.S. Wong, B. Benoit, M.D. Brand, Free Radic. Biol. Med. 130 (2019) 140–150.
[51] M.D. Brand, Free Radic. Biol. Med. 100 (2016) 14–31.
[52] M. Redza-Dutordoir, D.A. Averill-Bates, Biochim. Biophys. Acta 1863 (2016) 2977–2992.
[53] Y.X. Zhang, P.F. Yu, Z.M. Gao, J. Yuan, Z. Zhang, Eur. Rev. Med. Pharmacol. Sci. 21 (2017) 1665–1671.
[54] J. Kale, E.J. Osterlund, D.W. Andrews, Cell Death Differ. 25 (2018) 65–80.
[55] C. He, M.C. Bassik, V. Moresi, K. Sun, Y. Wei, Z. Zou, Z. An, J. Loh, J. Fisher, Q. Sun, S. Korsmeyer, M. Packer, H.I. May, J.A. Hill, H.W. Virgin, C. Gilpin, G. Xiao, R. Bassel-Duby, P.E. Scherer, B. Levine, Nature 481 (2012) 511–515.
[56] I. Tamm, Y. Wang, E. Sausville, D.A. Scudiero, N. Vigna, T. Oltersdorf, J.C. Reed, Cancer Res. 58 (1998) 5315–5320.
[57] K. Blomgren, C. Zhu, X. Wang, J.O. Karlsson, A.L. Leverin, B.A. Bahr, C. Mallard, H. Hagberg, J. Biol. Chem. 276 (2001) 10191–10198.
[58] A. Bressenot, S. Marchal, L. Bezdetnaya, J. Garrier, F. Guillemin, F. Plénat, J. Histochem. Cytochem. 57 (2009) 289–300.
[59] K. Zhang, S. Wu, H. Wu, L. Liu, J. Zhou, Aging (Albany NY) 13 (2021) 21090–21101.
[60] C.Y. Meng, Z.Q. Zhao, R. Bai, W. Zhao, Y.X. Wang, H.Q. Xue, L. Sun, C. Sun, W. Feng, S.B. Guo, Oncol. Rep. 43 (2020) 1169–1186.
[61] S.Y. Kim, H. Hwangbo, M.Y. Kim, S.Y. Ji, H. Lee, G.Y. Kim, C.Y. Kwon, S.H. Leem, S.H. Hong, J. Cheong, Y.H. Choi, Arch. Biochem. Biophys. 697 (2021), 108688.
[62] W. Yao, Z. Lin, P. Shi, B. Chen, G. Wang, J. Huang, Y. Sui, Q. Liu, S. Li, X. Lin, Q. Liu, H. Yao, Biochem. Pharmacol. 171 (2020), 113680.
[63] Z. Xu, X. Han, D. Ou, T. Liu, Z. Li, G. Jiang, J. Liu, J. Zhang, Appl. Microbiol. Biotechnol. 104 (2020) 575–587.